IPNO-DRE-94-22

VAPORIZATION OF THE Ar + Ni SYSTEM STUDIED WITH THE 4π MULTIDETECTOR INDRA

Ch.O. BACRI, B. BORDERIE, J.L. CHARVET,
R. DAYRAS, O. LOPEZ, A. OUATIZERGA, M.F. RIVET

Invited talk at CORINNE II.
International Workshop on Multi-Particle Correlations and Nuclear Reactions, Nantes (France)
6-10 sept 1994

VAPORIZATION OF THE Ar + Ni SYSTEM STUDIED WITH THE 4π MULTIDETECTOR INDRA

Ch.O. BACRI[3], B. BORDERIE[3], J.L. CHARVET[1], R. DAYRAS[1], O. LOPEZ[4], A. OUATIZERGA[3], M. F. RIVET[3]
G. AUGER[2], A. BENKIRANE[2], J. BENLLIURE[2], B. BERTHIER[1], R. BOUGAULT[4], R. BROU[4], P. BOX[3], Y. CASSAGNOU[1], A. CHBIHI[2], J. COLIN[4], D. CUSSOL[4], E. DE FILLIPO[1], A. DEMEYER[5], D. DURAND[4], P. ECOMARD[2], P. EUDES[6], A. GENOUX-LUBAIN[4], D. GOURIO[6], D. GUINET[5], L. LAKEHAL-AYAT[3], P. LAUTESSE[5], J.L. LAVILLE[6], L. LEBRETON[5], C. LEBRUN[4], J.F. LECOLLEY[4], A. LEFEVRE[2], R. LEGRAIN[1], M. LOUVEL[4], N. MARIE[2], V. METIVIER[4], L. NALPAS[1], M. PARLOG[3], J. PETER[4], E. PLAGNOL[3], E. POLLACO[1], A. RAHMANI[6], R. REGIMBART[4], T. REPOSEUR[6], E. ROSATO[4], F. SAINT-LAURENT[2], M. SQUALLI[3], J.C. STECKMEYER[4], B. TAMAIN[4], L. TASSAN-GOT[3], E. VIENT[4], C. VOLANT[1], J.P. WIELECZKO[2].

[1] *DAPNIA, CEN Saclay, 91191 Gif sur Yvette, France*
[2] *GANIL, BP5027, 14021 Caen, France*
[3] *Institut de Physique Nucléaire, IN2P3-CNRS, F91406 Orsay Cedex*
[4] *LPC, ISMRA, IN2P3-CNRS, 14050 Caen Cedex, France*
[5] *IPN Lyon, 69622 Villeurbanne Cedex, France*
[6] *SUBATECH, 44072 Nantes Cedex 03, France*

Abstract

Characterization of the nature of the deexcitation of highly excited nuclei through multi-fragment or particle emission requires the use of powerful multidetectors. In this spirit a broad program was undertaken which examines the multiple facets of multi-fragment emission with the multidetector INDRA. Results on the Ar+Ni system between 32 and 95 MeV/nucleon are presented, which evidence the production of a large number of fragments (up to 7) in central collisions, at all energies. Ultimately, the threshold for complete vaporization of the system into H and He isotopes is determined.

1 Introduction

One of the main goals of the current research in nuclear physics in the intermediate energy domain is to improve our knowledge about the properties of nuclear matter in extreme conditions of density and temperature. It is now well established that highly excited nuclear systems have a sizeable probability to decay by multi-fragment emission [1]. Whether this emission is a series of sequential binary break-ups or a "sudden multifragmentation" (accompanied or not by a phase transition) is one

of the most debated questions at the present time. Such a distinction might moreover be quite subtle due to the short time scales involved in both cases [2, 3]. The multifragmentation process is theoretically predicted to occur during the expansion of a hot and compressed system formed in the early stage of nucleus-nucleus central collisions [4, 5, 6]. While the compression has to be quite strong for light systems, a more gentle compression can be sufficient for very heavy systems as the expansion is there enhanced by the strong coulomb repulsion [7]. For systems with still higher excitation energies, vaporization is also predicted to occur, which is the disassembly of the system in very small pieces [8, 9].

Until recently, progress in the understanding of multi-fragment emission was partly hampered by the limitations of the available experimental devices. The 4π multidetector INDRA was built to efficiently study central collisions where large multiplicities of nuclei are observed in the exit channel. A broad program was undertaken by the INDRA collaboration to particularly study the influence of different parameters on the multifragmentation process. Among those parameters are the size of the system, the entrance channel characteristics (incident energy, mass asymmetry); Coulomb instabilities and the ultimate phase leading to the vaporization of the system are also searched for. The program also comprises the determination of the transverse flow of nuclear matter, which should bring information on the in-medium nucleon-nucleon cross section, and provide additional tests for the nuclear forces used in simulations [10]

This experimental program was worked out through two sets of experiments, the first one performed in 1993, and the second one in 1994. Fig. 1 displays the systems which were studied, and the specific parts of the program that each one adresses more specifically.

In the following, we will show results concerning only the Ar+Ni system; experimental details will be given in the next section. Then the evolution of the general trends with incident energy will be discussed, and finally we will present some data on vaporization events, which are, to our knowledge, observed for the first time below 100 MeV/nucleon.

2 The Ar + Ni system - Experiment

The experiments were performed at GANIL, using the 4π multidetector INDRA. A brief description of the detector will be given, more details can be found in ref[11, 12].

2.1 The 4π multidetector INDRA

INDRA is a 4π multidetector designed to detect charged products. It has a high geometrical efficiency of 90% of 4π and very low detection thresholds. Operated under vacuum, the detector is composed of 336 independent modules shared between 17 rings symmetric around the beam axis. A general view of the detector is schematized

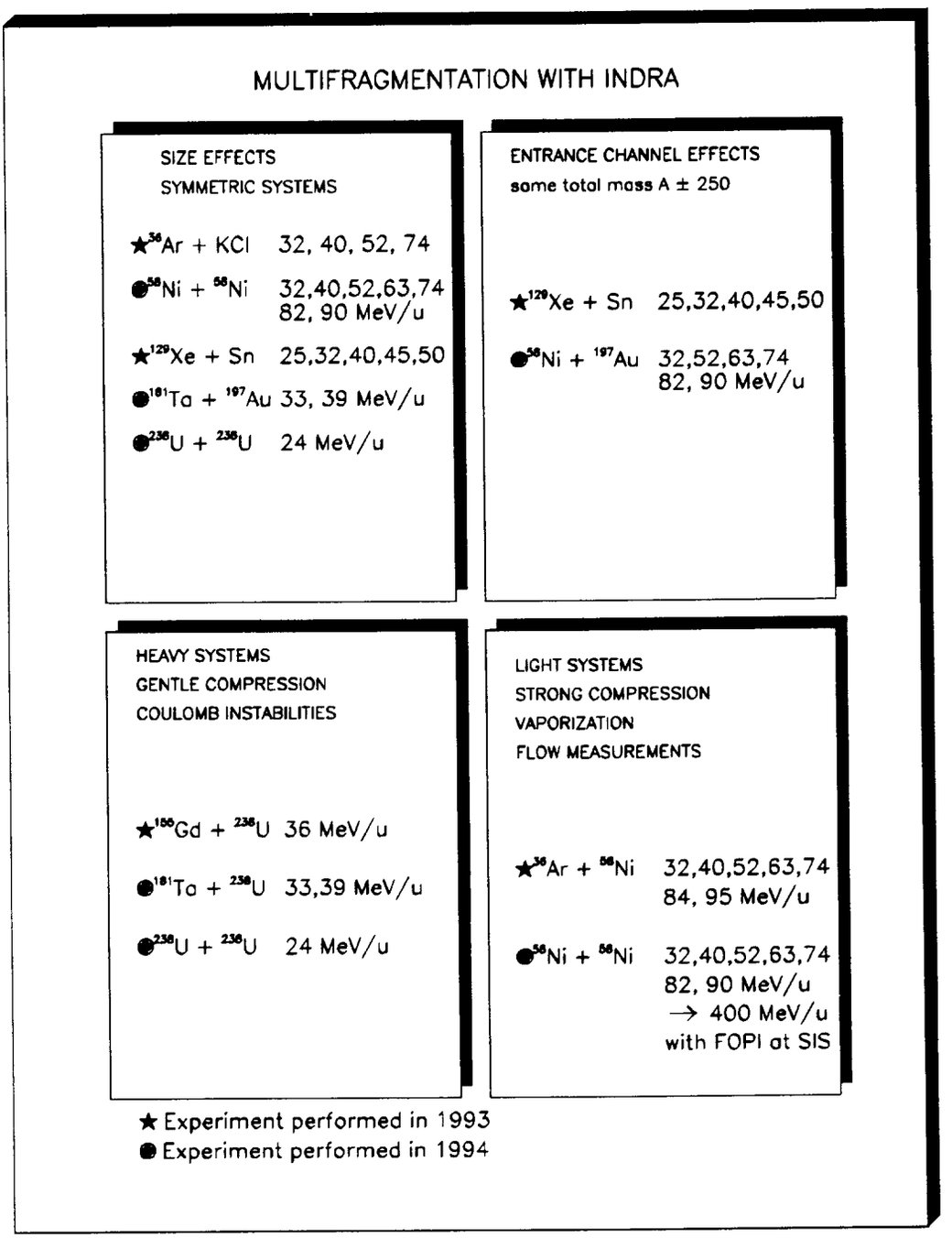

Figure 1: *The experimental program realized with INDRA.*

in fig. 2.

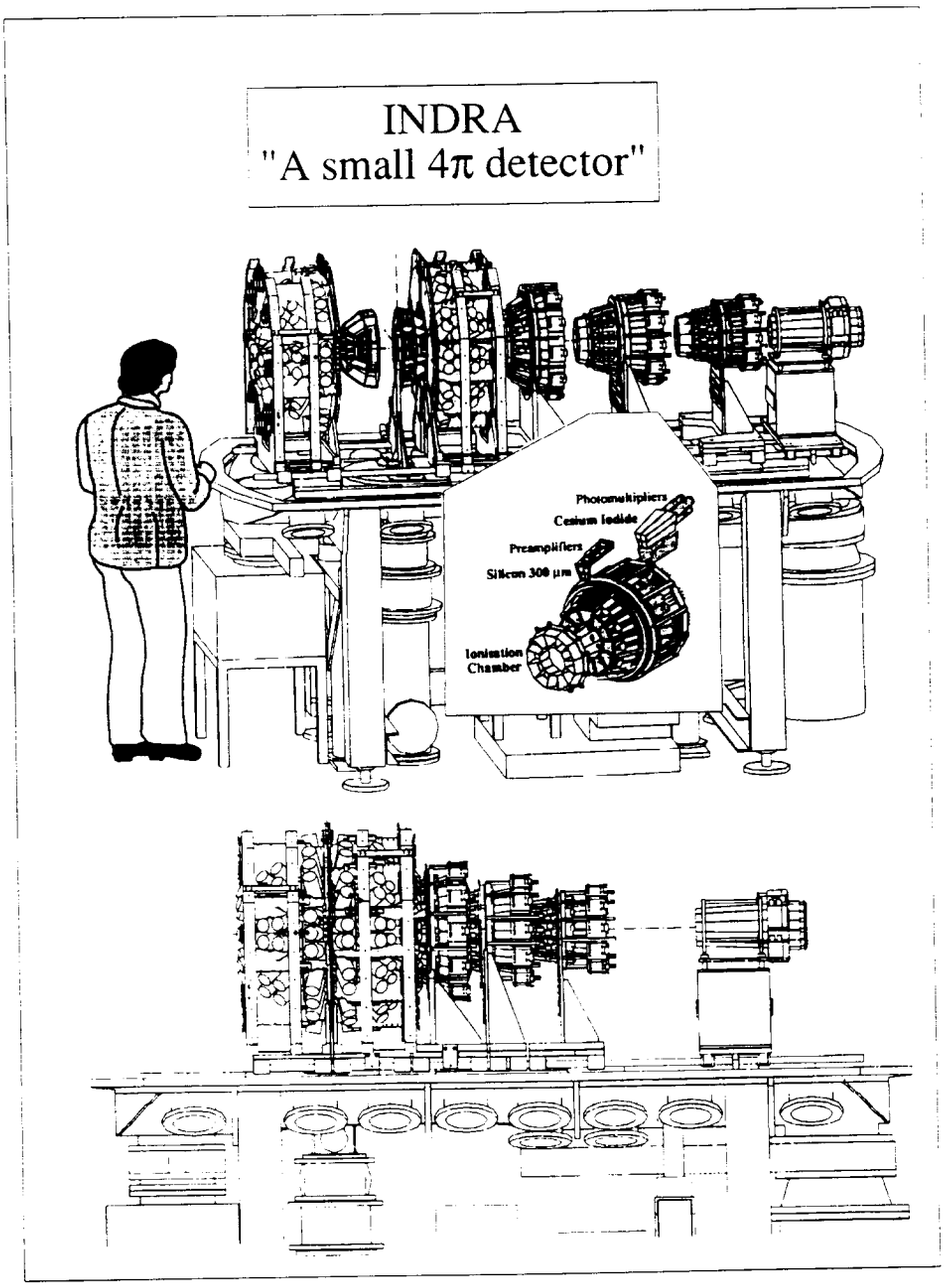

Figure 2: *Schematic view of INDRA. Bottom: running configuration. Top: open configuration, and detail of a forward module.*

The basic modules comprise two or three stages, depending on angle, for complete identification of products on a large energy range; low energy thresholds for fragments

are insured, on rings 2-17, by an ionization chamber operated with low pressure C_3F_8 gas. Light particle mass separation is based on pulse shape analysis of the signals of CsI scintillators coupled to photomultiplier tubes (rings 2-17). A $300\mu m$ silicon detector is placed between these two layers for rings 2-9 ($\theta = 3 - 45^o$), where low energy particles and fragments issued from the target coexist with beam velocity particles and fragments from the projectile. Finally at very forward angles the first ring ($\theta = 2-3^o$) is composed of fast plastic phoswiches, which can endure the expected high flux of elastically scattered particles. For calibration purposes, a two-member telescope (80μ Si + 2 mm Si(Li)) was inserted in front of one of the CsI of rings 10-17, which do not incorporate silicon detectors.

The huge dynamical energy range to cover ($\sim$5000) made it necessary to replace the traditional amplitude encoding by a charge encoding for silicon and ionization chambers signals. The large number of detectors to handle led to the development of a highly integrated electronics, using the new VXIbus standard. Full remote control of parameter settings, including visualization of signals is thus allowed.

2.2 Experimental conditions

The 95 MeV/nucleon ^{36}Ar beam was delivered by the GANIL accelerator. Other energies were obtained by slowing down this beam, further analyzed by the "alpha magnetic spectrometer" of GANIL. In order to keep the rate of random coincidences as low as possible, beam intensities were maintained very low, typically 3-4 10^7 pps. A unique 193 $\mu g/cm^2$ ^{58}Ni target was used at all bombarding energies. The backward ionization chamber of INDRA was not installed during these experiments, preventing the separation of low energy fragments ($Z \geq 3$) and He isotopes at angles larger than 90^o.

For this first set of measurements, a minimum bias trigger was chosen, namely a multiplicity value. Events were registered when at least 3(4) modules fired for the energies 32-74 (84-95) MeV/nucleon; In these conditions the dead time of the acquisition system was around 20%. In this paper, absolute cross sections will be calculated from the target thickness and the number of impinging Ar ions, taking into account the dead time. For normalization purposes, some tapes were registered without any bias (multiplicity ≥ 1). At 52 MeV/nucleon we could thus verify that the total measured cross section was within 10% of the value predicted by the systematics on reaction cross sections established by Kox et al [13].

2.3 Data treatment

At the present time complete charge identification is achieved for the experiments performed in 1993. We define a "fragment" as having a charge $Z \geq 3$ and a light charged particle (lcp) as a hydrogen or a helium isotope. The identification includes tests for the consistency of the responses of all detection layers passed through by

a particle. In some cases this procedure allows to separate particles piled-up in one module; typically one can separate a fast light charged particle fully identified in the CsI scintillator from any slow particle stopped in the preceding silicon detector.

The presence of a silicon detector at forward angles (up to 45°) gives full charge and mass identification over the whole energy range for elements up to Boron. Charge identification alone is achieved for heavier elements, up to at least xenon (Z=54) for nuclei reaching the CsI, and up to Z=27 for nuclei stopped in the silicon detector.

At backward angles, the ionization chamber insures charge separation near the detection threshold for lcp, and over the whole energy range for heavier fragments. Mass identification is obtained only from the CsI response, and is typically achieved above 5 MeV for deuterons and 10 MeV for tritons. Separation between ^3He,^4He,^6He occurs around 25 MeV.

Examples of the performances of INDRA for particle identification can be found in [12], together with the methods used for energy calibrations. These calibrations are still in progress, and therefore only data concerned with the numbering of the identified particles will be presented in the following.

3 Evolution of the Ar + Ni system between 32 and 95 MeV/nucleon: general features

A global view of the results obtained for the Ar + Ni system is shown in fig. 3.

It represents the total detected charge (Z_{tot}, sum of the charges of all identified particles) versus the multiplicity of charged products, for 6 out of the 7 studied energies. The first remarkable feature is the quality of the detection: for all energies, there are quite a number of events for which a large fraction of the total charge of the system (Z = 46) is detected. Moreover this efficient detection covers a large range of multiplicity, from about 10 up to the highest multiplicity value. This demonstrates that INDRA is indeed well suited for studying central collisions, where a large number of fragments and of light charged particles are emitted. As expected, the maximum measured multiplicity increases with the incident energy, from 25 at 32 MeV/nucleon to 35 at 95 MeV/nucleon.

Now one can also distinguish, at all energies, two regions where events are not well measured. Both are in the low multiplicity range, the first one starting at $Z_{tot} = 1$ (region 1), and the second one at $Z_{tot} \sim 18$ i.e. the charge of the projectile (region 2). From what is known about the reaction mechanisms intervening in peripheral collisions in the energy domain 10-100 MeV/nucleon[14], one can infer that we are here dealing with dissipative collisions, with essentially two fragments and light charged particles in the exit channel. In the first region we miss both the target-like fragment (TLF) and the projectile-like fragment (PLF). In the second one the PLF is detected, but not the TLF. This hypothesis is confirmed when looking at the evolution of the charge of the biggest detected fragment versus the multiplicity (fig. 4 bottom).

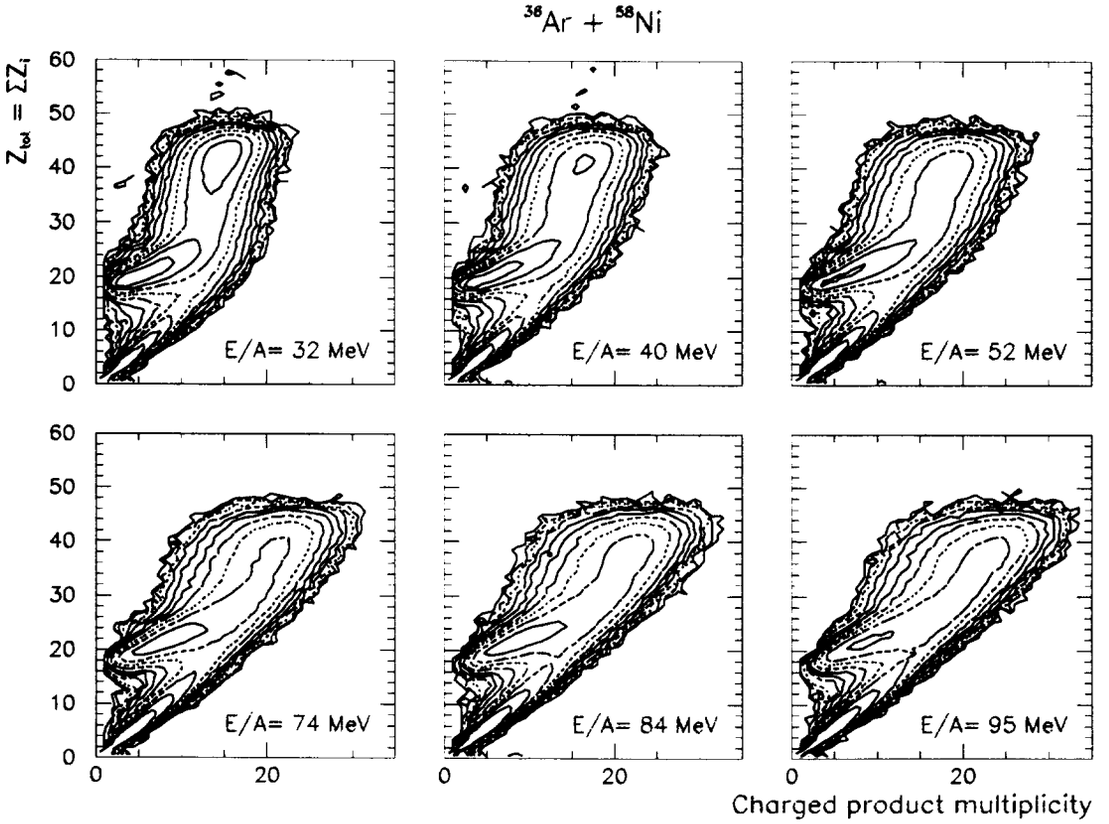

Figure 3: *Evolution of the total detected charge as a function of the charged product multiplicity. The total charge of the system is* $Z_{tot} = 46$.

Indeed, starting from low multiplicity values, one sees two ridge lines: the first one is located at $Z_{max} \sim 2 - 3$, and corresponds to region 1 defined above; the second ridge, beginning at the projectile charge and going toward lower Z values when the multiplicity increases, can be associated with the PLF; this evolution reflects the increasing excitation energy of the PLF. Another region appears in these maps for high multiplicities(around 15-20), which extends to $Z_{max} \sim 30$ at 32 MeV/nucleon, and still to Z_{max} as large as ~ 20 at the higher bombarding energies. Without further information, one can speculate that some incomplete fusion events are observed at the lowest energies (32 and 40 MeV/nucleon). We may also have evidenced the existence of "sun events" [15]in which one large fragment subsists among smaller ones; such events should be very rare, and indeed the presence of a large fragment at high multiplicities occurs only in the tail of the Z_{max} distributions.

Let us play now the game of "reconstructing" the peripheral events (in average):

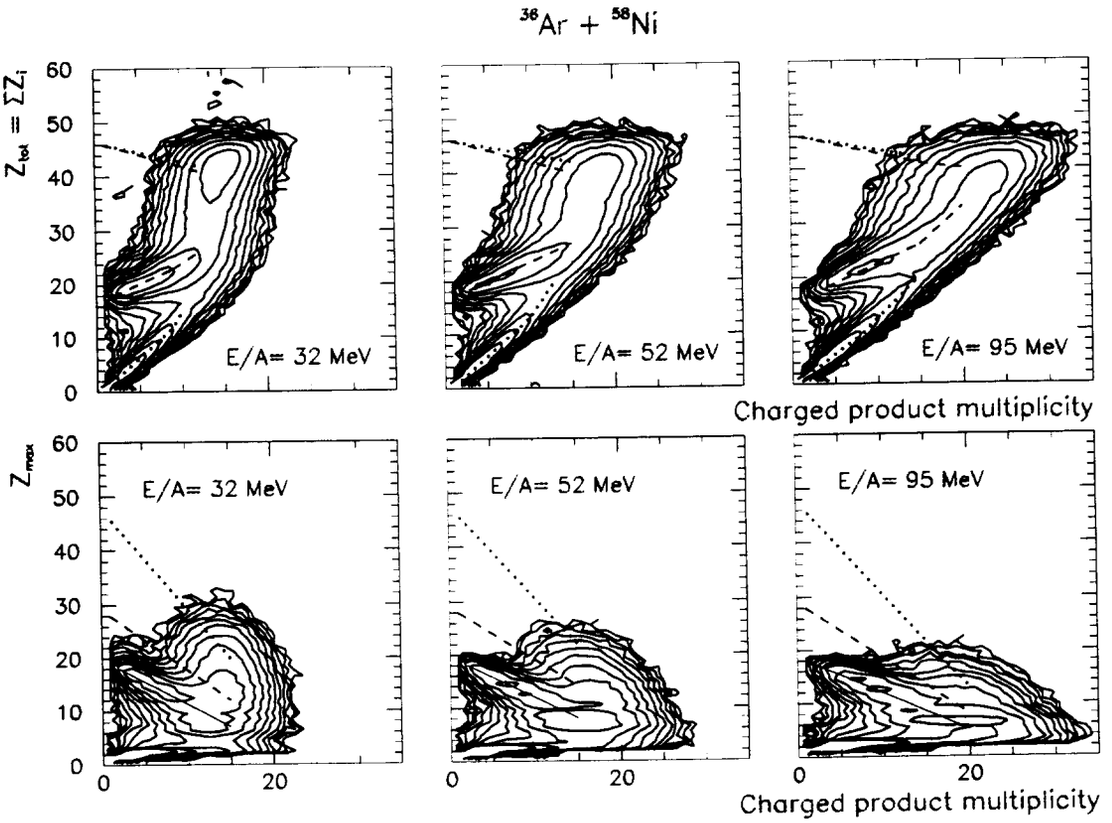

Figure 4: *Top: same as fig. 3 for 3 incident energies. Bottom: Evolution of the charge of the biggest detected fragment as a function of the charged product multiplicity for the same energies.*

First we deduce the average ridge line of the TLF by scaling the measured line for the PLF by the ratio of the charge of the target to that of the projectile (fig. 4 bottom). Then we go back to the picture representing the total detected charge (fig. 4 top): to the average value of Z_{tot} in region 2 we add the deduced average charge of the TLF (dashed lines); to the average value of Z_{tot} in region 1 we add the deduced summed charges of the TLF and the PLF (dotted lines). In both cases we end up at total "reconstructed" average charges around 90% of the charge of the system. This means that in peripheral collisions INDRA indeed misses one, or the two partners of the binary reaction, for kinematical reasons, but that it detects most of their deexcitation products, the limit being the geometrical efficiency of the detector.

Another general feature of the reaction is the evolution of the number of frag-

ments versus the multiplicity, for the incident energy range studied, represented in fig. 5. For all energies the number of fragments increases with the multiplicity, the maximum observed value being 7 fragments. Moreover the projected fragment number distributions are quite similar at all energies; the average size of the fragments is however a decreasing function of the incident energy, due to charge conservation [16]: if the number of fragments remains constant while the number of lcp increases, then the size of the fragments has to decrease. The lack of selectivity of the incident energy on the number of fragments is quite intriguing, and will be examined in more details when the energy of the detected products will be known.

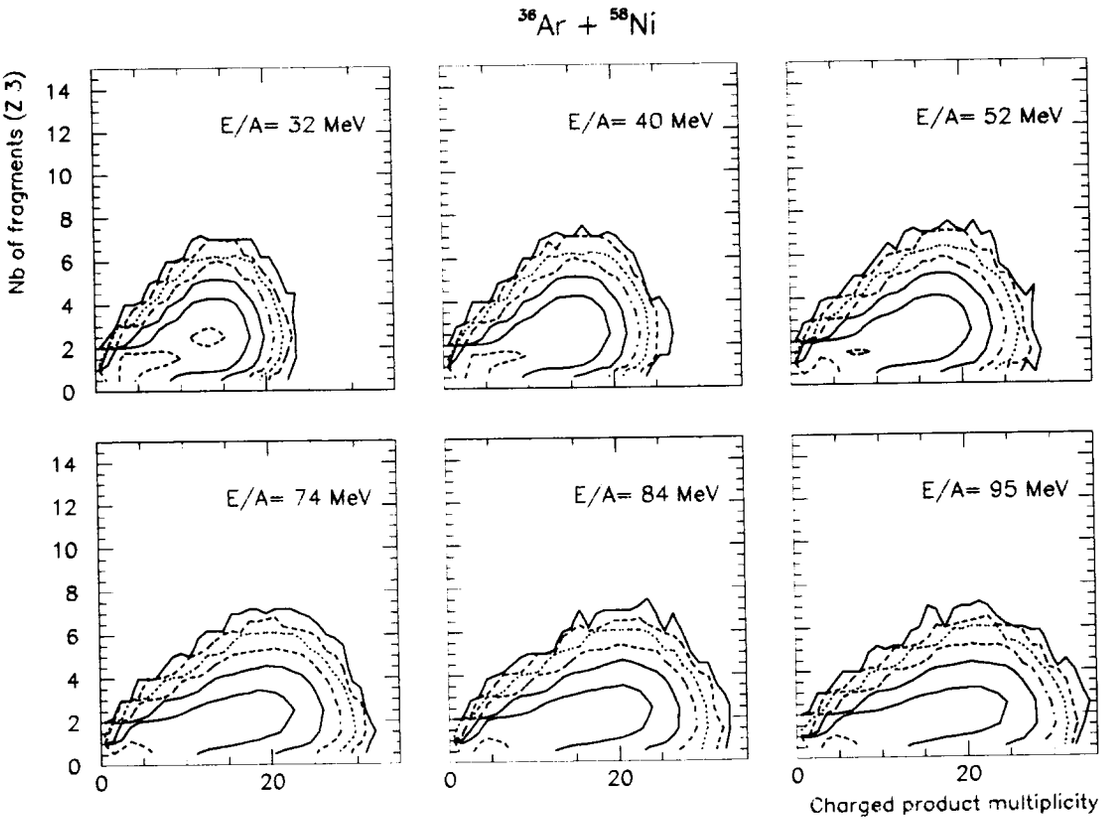

Figure 5: *Evolution of the number of fragments as a function of the charged product multiplicity, for 6 different energies.*

4 Vaporization events

4.1 Definition and selection

In this section, we will skip over multifragment emission, and examine a class of events which we call "vaporization events". They are defined as the events containing only light charged particles, without any assumption on the intervening mechanisms. This is a very drastic definition, as for instance some theoreticians allow "vaporization events" to contain several fragments providing their mass is small enough [8, 9].

The question is how to correctly select such events (keeping in mind that up to now we can only rely on charge measurements). The safer way would be to only keep events where the total charge of the system is detected, with a tolerance of one helium missing. The statistics would then be too poor. Therefore we enlarge our selection, and search for events for which the probability to have detected *all* fragments is 90%; then when we will require events containing zero fragment, we will be quite sure that so did the true complete event. The method of selection is based on a "simulation" using the experimental data, and is sketched in fig. 6 for the highest incident energy:

First we keep only events for which the total charge measured is at least the projectile charge (i.e. we eliminate the region 1 defined in the previous section). For these events we divide the multiplicity distribution in 5 bins as indicated in fig. 6a; the charge distribution is determined for each bin (fig. 6c). Note that in all cases lcp largely dominate (the yield drops by a factor of 10 between Z=2 and Z=3). For the lower multiplicity bin the charge distribution extends up to Z $\sim$25, after exhibiting a plateau between Z = 3 and Z$\sim$11. For higher multiplicities, the charge distribution becomes steeper and steeper.

For each multiplicity bin:

i)We assume that the true charge distribution is similar to the measured one.

ii) We construct complete events (Z_{tot} = 46), by random sampling on the charge distribution. This gives a calculated multiplicity

iii) We go back to the measured multiplicity (weigthed by the experimental distribution) by discarding the appropriate number of particles at random (assuming that the probability of losing any particle is the same). The reconstructed map Z_{tot} versus multiplicity is shown in fig. 7b together with the measured one. The two maps are similar enough to valid the selection method.

iv) We search for events which the probability to have detected all fragments is 90% (whatever the initial number is), which sets a limit on the total detected charge: It turns out that at all incident energies this limit is quite independent of the multiplicity, and equal to Z_{tot} = 41, as appears in fig. 7c.

What range of reactions do we explore with such a selection? This is shown on the multiplicity distributions, fig. 7d. There are displayed the multiplicity distributions we started with (total detected charge larger than the projectile charge), then those

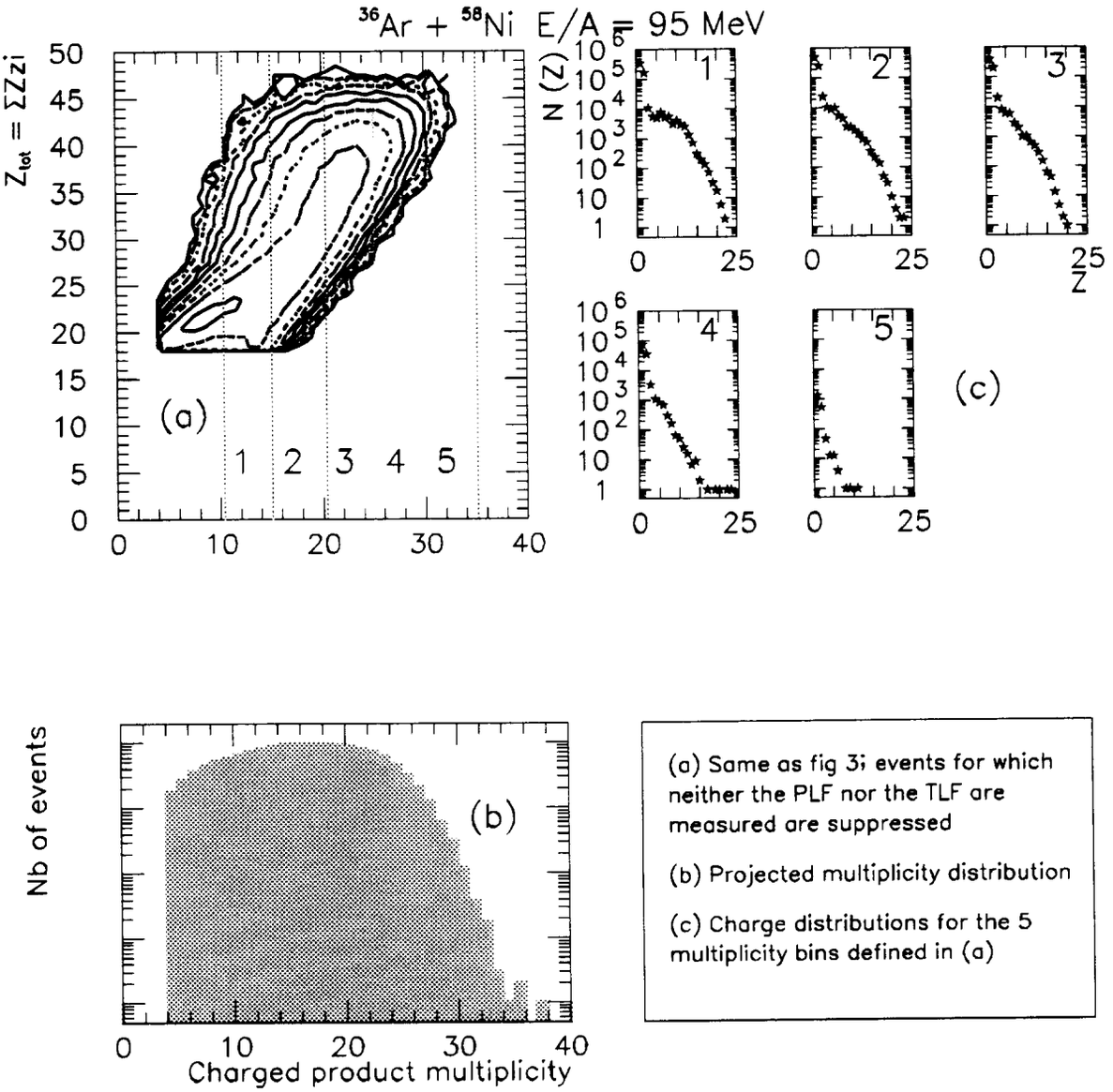

Figure 6: *Method used for selecting vaporization events.*

obtained with the limit $Z_{tot} \geq 41$. Obviously this limit selects the highest multiplicities, but explores quite a large range of the initial distribution. If we put on top of the multiplicity scale an impact parameter scale, the explored zone corresponds to 70% of the grazing impact parameter. The impact parameter scale is here a rough estimate based on the multiplicity distribution, assuming a unique correspondance

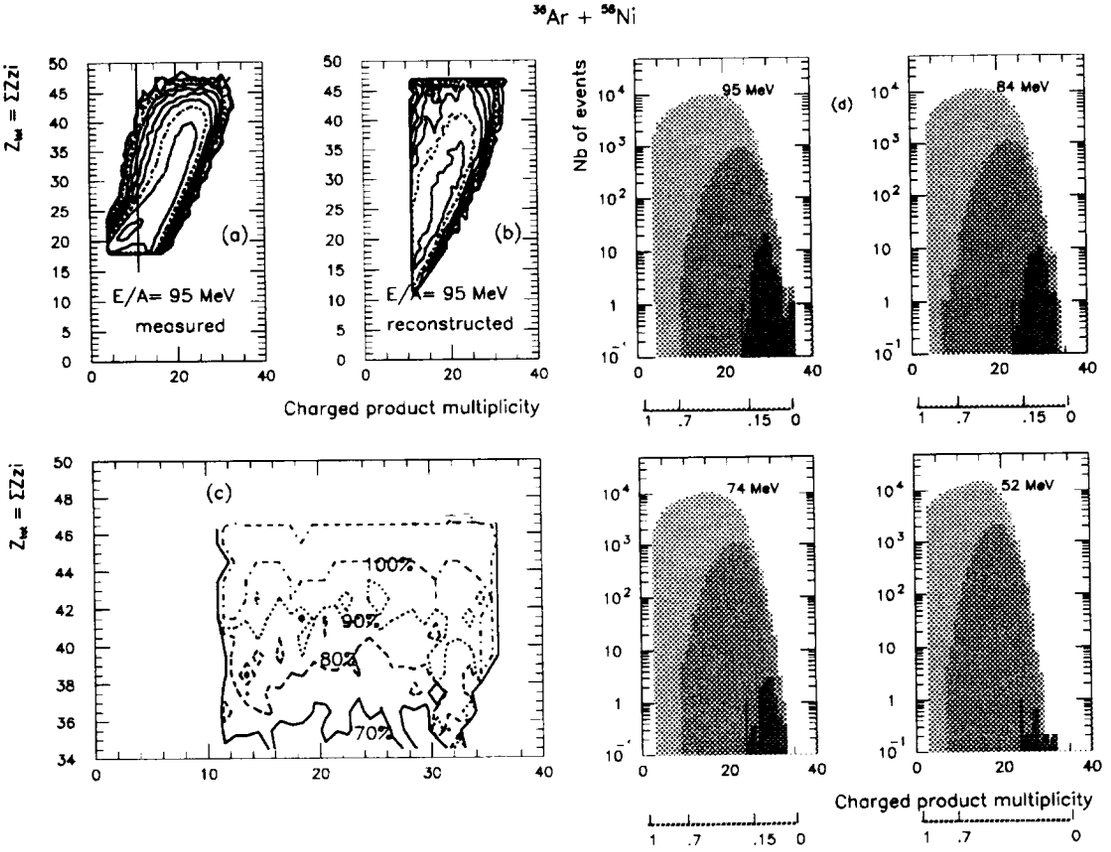

Figure 7: *a,b,c, Total detected charge versus charged product multiplicity: a) experimental map, same as fig. 6a; b) Reconstructed map to be compared to the events to the right of the vertical line in (a); c) Events with a given probability to have detected all fragments; d) Multiplicity distributions; for each energy, the highest one corresponds to the projection of fig. 6a; the next one includes the selection* $Z_{tot} \geq 41$. *The smaller one displays the distribution for the vaporization events. An impact parameter scale (relatively to the grazing impact parameter) is given below.*

between a multiplicity value and an impact parameter, and the grazing impact parameter is deduced from calculated reaction cross sections [13]. Not shown here is the effect of the selection $Z_{tot} \geq 41$ on the size of the biggest fragment: clearly the part corresponding to a PLF resulting from peripheral or mid-peripheral collisions is suppressed [16]. The number of remaining events represents $\sim 5\%$ of the measured events (i.e. those with a multiplicity above the triggering value) for incident energies above 50 MeV/nucleon.

If we finally turn to the vaporization events, which are now defined as those for which the total detected charge amounts at least to 41, and which contain no frag-

ment, their multiplicity distribution is also displayed in fig. 7d. They are evidently located in the highest multiplicity region (our definition implies that at least 23 particles should be detected, if they were all He isotopes!), and therefore should originate from rather central collisions. It was verified that these rare events, located in the very tail of the multiplicity distributions do not result from pile-up events.

4.2 Excitation function and structure of the events

The first information which can be extracted is the cross section of such events. None were found for incident energies below 52 MeV/nucleon. Above this energy the excitation function rises sharply, while never exceeding some 10^{-4} times the reaction cross section (fig. 8). We can therefore infer that the threshold for vaporization events is, for this system, around 50 MeV/nucleon.

Next we can examine the composition of these events. For this we have plotted in fig. 8 the average proportion per event of each measured isotope with respect to the measured charged particle multiplicity. The most abundant particles are the α's, which exhaust half of the measured multiplicity at 52 MeV/nucleon. Their relative yield decreases when the incident energy increases, showing that when more energy is available, the tendancy is to break the system in smaller and smaller pieces. This very abundant production of α particles might originate in the structure of the chosen incident nuclei: ^{36}Ar can be viewed as a cluster of 9 α particles, and ^{58}Ni as 14 α particles and 2 neutrons. It would be interesting to study similar events on systems where the incident nuclei would be for instance neutron rich. While the relative proton yield remains constant, the decreasing proportion of α's seems to be replaced essentially by deuterons. The abundance of other loosely bound isotopes, tritons and ^{3}He increases only slightly between 52 and 95 MeV/nucleon. The relative abundance of ^{3}He is slightly smaller than that of tritons. This may be due to experimental identification thresholds at backward angles (see section 2.3), and will be verified later by putting gates on the particle energies.

4.3 Energetics

As mentioned earlier, we do not know yet precisely the energy of the detected particles, but we tried anyway some speculations on the energetics of the reaction. This is shown in fig. 9 where is firstly plotted the available energy per nucleon, which increases from 12 to 22 MeV in the explored lab. energy range.

Then each of the measured event is "completed" in charge and mass with protons and neutrons. The mass balance of the reaction is then readily obtained. Charged particles cannot be emitted without kinetic energy, but have at least the Coulomb repulsion. It was calculated by putting all the particles of each event in a close configuration, and letting them go to infinity under the action of the Coulomb force. The sum of the mass balance and of the Coulomb energy amounts to 6-7 MeV/nucleon

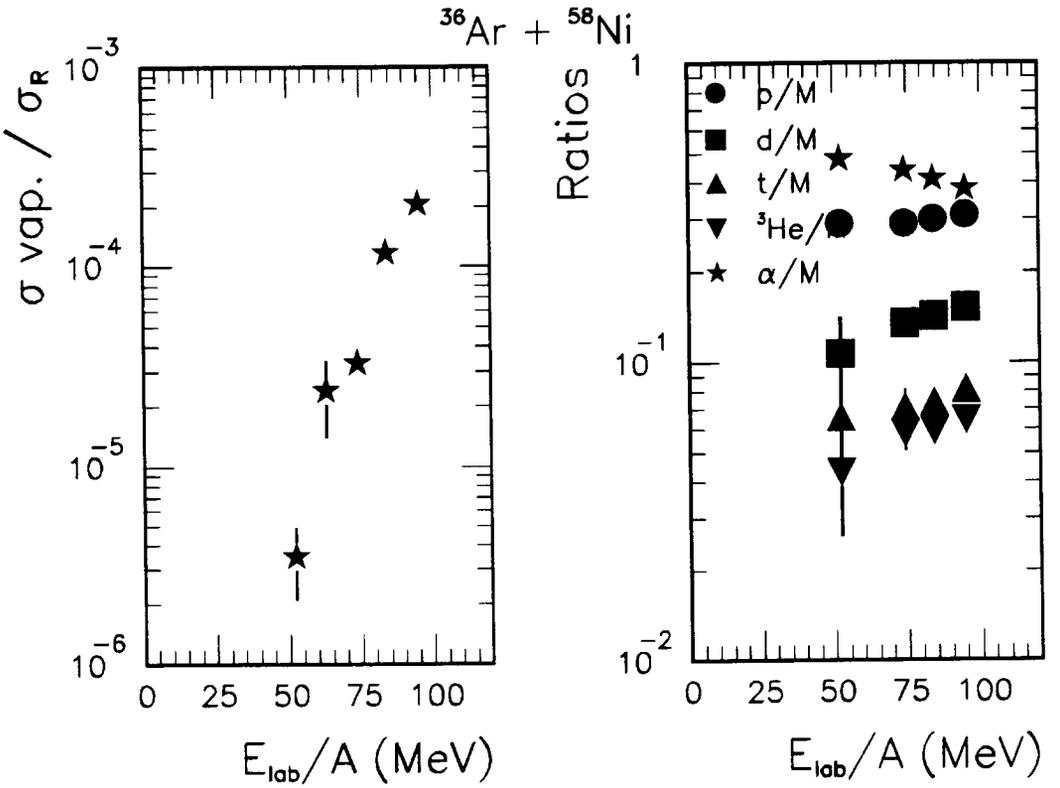

Figure 8: *Left: Excitation function for the vaporization events. Cross sections are normalized on calculated reaction cross sections (see text). Right: average proportions of the different particle species in the vaporization events.*

(the plotted quantities are averages over all events). This quantity has to be available. We can now speculate that each particle has also a part of its kinetic energy coming from thermal energy, which would then be twice the temperature if the system is equilibrated before breaking. By refering to the highest measured temperature in central collisions on the Ar+Al [17]and Ar+Ag [18]systems, whose masses bracket that of the studied system, we assume a temperature of 7 MeV, at all incident energies. The excitation energy of the system then reads:

$$\epsilon^* = (Q + V_c + 2 * M_{corr} * T)/A_{tot}$$

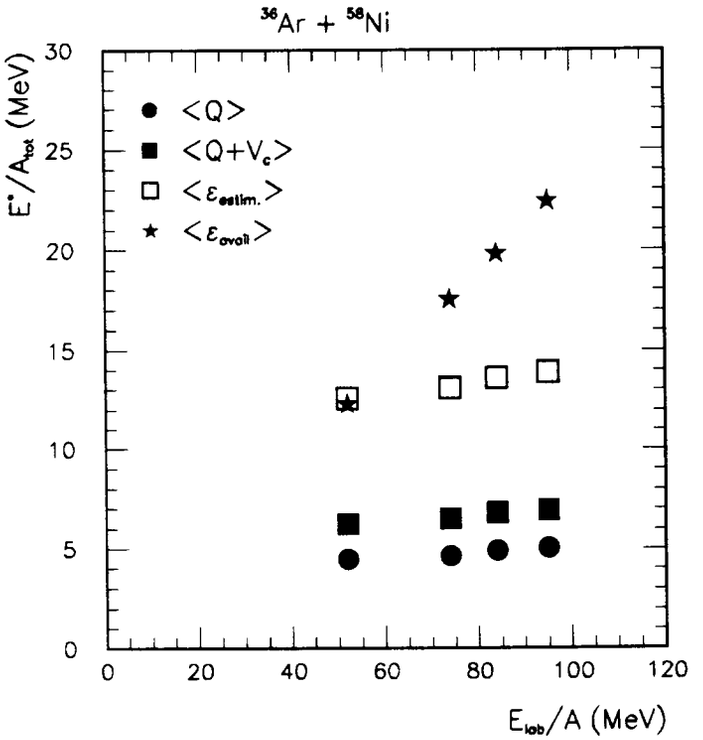

Figure 9: *Plot of the different components which enter the estimated excitation energy of the system (see text).*

where V_c is the Coulomb energy, M_{corr} the corrected particle multiplicity (including neutrons) and $A_{tot} = 94$ the total mass of the system.

When plotting the values so estimated for the excitation energy, it apppears that for 52 MeV/nucleon incident energy, the excitation energy is just equal to the available energy, which would explain why we find here the threshold for vaporization. Evidently, it only means that in the excitation energy distribution of the system, a very small fraction is stored in such a form that it allows this break-up to take place. This fraction is then increasing with the available energy. Here again, more precise conclusions will be given when the center of mass energy and angular distributions of the particles will be known.

References

1. L.G. Moretto and G.J. Wozniak, *Annual Rev. of Nucl. and Part. Science* **43** (1993) 379 and references therein.
2. B. Borderie, *Ann. Phys. Fr.* **17** (1992) 349.
3. A.S. Botvina and D.H.E. Gross, *Preprint HMI* (1994)
4. J. Cugnon, *Phys. Lett.* **B135** (1984) 374.
5. G.F. Bertsch and Ph. Siemens, *Phys. Lett.* **B126** (1989) 9.
6. E. Suraud et al., *Nucl. Phys.* **A495** (1989) 73c.
7. B. Borderie et al., *Phys. Lett.* **B302** (1993) 15.
8. J. Bondorf et al, *Phys. Lett.* **162B** (1985) 30.
9. D.H.E. Gross, Zhang Xiao-ze and Xu Shu-yan, *Phys. Rev. Lett.* **56** (1986) 1544.
10. V. de la Mota et al., *Phys. Rev.* **C46** (1992) 677.
11. B. Borderie, *XXXI Int. Winter Meeting on Nucl. Phys., Bormio*, ed. I. Iori (Ricerca Scientifica ed Educazione Permanente 1993), p. 238. E. Plagnol et al, *Nouvelles du GANIL* **44** (feb. 1993).
12. J. Pouthas et al, submitted to *Nucl. Inst. Meth.* (1994)
13. S. Kox et al, *Nucl. Phys.* **A420** (1984) 162.
14. B. Borderie, M.F. Rivet and L. Tassan-Got, *Ann.Phys.Fr.* **15** (1990) 287 and references therein.
15. O. Schapiro and D.H.E. Gross, *Nucl. Phys* **A576** (1994) 428.
16. F. Saint-Laurent for the INDRA collaboration, *Proceedings of the Fifth Int. Conf. on Nucleus-Nucleus Collisions, Taormina, Italy* and Preprint GANIL P 94-25 (1994).
17. D. Cussol et al., *Nucl. Phys.* **A561** (1993) 298.
18. M.F. Rivet et al, *XXXI Int. Winter Meeting on Nucl. Phys., Bormio*, ed. I. Iori (Ricerca Scientifica ed Educazione Permanente 1993), p. 92.